

NODAL COARSENING AND SPARSE IDEAL INTERPOLATION FOR $H(\text{curl})$ PROBLEMS IN ALGEBRAIC MULTIGRID

TAOLI SHEN*, JAMES BRANNICK†, ROBERT FALGOUT‡, KARSTEN KAHL§, AND JACOB SCHRODER¶

Abstract. We propose a sparse interpolation construction and a practical coarsening algorithm for the algebraic multigrid (AMG) method, tailored towards $H(\text{curl})$. Building on the generalized AMG framework, we introduce an interior/exterior splitting that yields both a refinement-based and a fully algebraic construction of the interpolation. The refinement-based approach follows geometric hierarchy, while the purely algebraic interpolation is constructed through a coarsening process that first coarsens a nodal dual problem and then builds coarse and fine variables using a matching algorithm. We establish the weak approximation property and the commuting relation under certain assumptions. Combined with matching block smoothers, the proposed interpolation yields an effective algebraic multilevel method. Numerical experiments show robustness under strong coefficient jumps, where the proposed methods substantially outperform standard geometric multigrid.

Key words. algebraic multigrid, ideal interpolation, $H(\text{curl})$, de Rham complex

1 Introduction Algebraic multigrid (AMG) is an algorithm for solving linear systems of equations typically derived from the discretization of a partial differential equation,

$$(1.1) \quad \mathbf{A}\mathbf{u} = \mathbf{f},$$

where $A \in \mathbb{R}^{n \times n}$ is a sparse matrix. AMG constructs a fast solver through a complementary process of relaxation and coarse-grid correction. The basic approach in AMG is to identify the smooth error (i.e., error not effectively reduced by relaxation) and then coarsen and build interpolation that directly approximates and treats such error. For scalar systems, one assumes the constant represents smooth errors locally, and this assumption is the key to the design of classical AMG [8].

However, classical injection-based AMG is inadequate for $H(\text{curl})$ problems with large near-kernel. In this work, we propose a sparse approximation of the ideal interpolation tailored to $H(\text{curl})$ problems. Unlike the topological constraint-based AMG approach by Reitzinger and Schöberl [7], our construction is derived from the ideal interpolation framework, allowing us to leverage the generalized AMG (GAMG) [2] convergence theory directly. Compared to recent global energy-minimization approaches [9], our approach achieves jump-robustness through a local harmonic extension while remaining sparse and computationally lightweight.

Next, we introduce the GAMG theory. The two-grid AMG scheme is summarized by the error propagator

$$(1.2) \quad E_{TG} = (I - M^{-1}A)(I - \Pi_A(P)),$$

where M defines the smoother, $P \in \mathbb{R}^{n \times n_c}$ denotes the interpolation matrix that maps error corrections to the fine level, $A_c := P^T A P$ is the Galerkin coarse-grid matrix,

*Department of Mathematics, The Pennsylvania State University, University Park, PA 16802, USA (tzs5765@psu.edu)

†Department of Mathematics, The Pennsylvania State University, University Park, PA 16802, USA (jjb23@psu.edu)

‡Lawrence Livermore National Laboratory, Livermore, CA 94550, USA (falgout2@llnl.gov)

§Fachgruppe Mathematik & Informatik, Bergische Universität Wuppertal, 42119 Wuppertal, Germany (kkahl@uni-wuppertal.de)

¶Department of Mathematics & Statistics, University of New Mexico, Albuquerque, NM 87106, USA (jbschroder@unm.edu)

and $\Pi_A(P) = PA_c^{-1}P^T A$ is the A -orthogonal projection of P . One of the main goals of this paper is to define a proper splitting of the degrees of freedom (DoFs) into coarse and fine.

Assuming that the system matrix A is symmetric, the generalized AMG two-grid theory can be summarized as follows [2, 3, 1].

$$(1.3) \quad \|E_{TG}\|_A^2 \leq 1 - \frac{1}{K}, \quad \text{where} \quad K := K(PR) = \sup_{\mathbf{e}} \frac{\|(I - PR)\mathbf{e}\|_{\widetilde{M}}^2}{\|\mathbf{e}\|_A^2} \geq 1,$$

where $\widetilde{M} = M(M + M^T - A)^{-1}M^T$ is the symmetrized smoother. Here, $R : \mathbb{R}^n \mapsto \mathbb{R}^{n_c}$ is any matrix for which $RP = I_c$, the identity on \mathbb{R}^{n_c} , so that PR is a projection onto $\text{range}(P)$. The derivation of the GAMG theory [2] which we use to design our AMG solver begins with the ℓ_2 -space decomposition of $V = \mathbb{R}^n = \text{span}(S) \oplus \text{span}(R^T)$ into a basis for the fine variables, the columns of the matrix $S \in \mathbb{R}^{n \times n_s}$, and a basis for the coarse variables, the columns of the matrix $R^T \in \mathbb{R}^{n \times n_c}$. If we assume the orthogonality conditions $RS = 0$, $S^T S = I_s$, and $RR^T = I_c$ as in GAMG, then

$$(1.4) \quad \mathbf{u} = Q_S \mathbf{u} + Q_R \mathbf{u} = S \mathbf{u}_s + R^T \mathbf{u}_c, \quad Q_S = SS^T, \quad Q_R = R^T R,$$

with \mathbf{u}_s denoting the fine variables and \mathbf{u}_c the coarse variables in these new bases. The corresponding ideal interpolation used as motivation is then:

$$(1.5) \quad P_\star := \arg \min_{P: RP=I_c} K(PR) = \begin{bmatrix} S & R^T \end{bmatrix} \begin{bmatrix} -(S^T AS)^{-1}(S^T AR^T) \\ I \end{bmatrix} \\ = (I - S(S^T AS)^{-1}S^T A)R^T.$$

This form of ideal interpolation gives a global harmonic extension in these new bases that minimizes the two-grid convergence rate for a fixed smoother.

2 The Curl-Curl Equation

Consider the shifted definite curl-curl equation

$$(2.1) \quad \begin{aligned} \nabla \times (\mu^{-1}(x) \nabla \times \mathbf{u}) + \beta \mathbf{u} &= \mathbf{f} \quad \text{in } \Omega, \\ \mathbf{u} \times \mathbf{n} &= 0 \quad \text{on } \partial\Omega, \end{aligned}$$

where $\beta > 0$ is small, $\Omega \subset \mathbb{R}^d$, and $\mu^{-1}(x)$ is piecewise constant and may exhibit large jumps across interfaces. Discretizing (2.1) with lowest-order Nédélec edge elements [6, 5] yields the SPD system

$$A\mathbf{u} = \mathbf{f}, \quad A = A^s(\mu) + \beta A^m,$$

where $A^s(\mu)$ and A^m denote the curl-curl stiffness and mass matrices, respectively. By the de Rham complex, the stiffness matrix satisfies

$$(2.2) \quad \ker(A^s(\mu)) = \text{range}(G),$$

where G is the discrete gradient mapping from the nodal space to the edge space. As $\beta \rightarrow 0$, A becomes increasingly ill-conditioned and exhibits a large $O(n)$ near-kernel. Therefore, non-pointwise smoothers [4] are needed for an optimal multigrid method.

2.1 AMG interpolation for curl-curl The construction of our AMG interpolation is motivated by the ideal interpolation operator defined in (1.5). In classical AMG, the coarse and fine variables, R and S , take the form

$$(2.3) \quad R = [0 \quad I], \quad S = \begin{bmatrix} I \\ 0 \end{bmatrix}$$

It is clear that this type of coarsening simply injects a subset of fine DoFs into the coarse mesh, which is highly inaccurate for preserving near-kernel structures. In fact, with this choice of R and S , even under robust block smoothers, linear combinations of overlapping gradient modes are not accurately represented on the coarse grid when simple injection is used, which leads to convergence stagnation. Instead, as demonstrated in [7, 9], a key property for robust multilevel convergence for curl-curl is to satisfy the commuting property

$$(2.4) \quad PG_c = GP_n$$

where G_c is the coarse level gradient and P_n is some nodal interpolation. Therefore, when defining coarse variables, it is essential to preserve the correct oriented averaging of local near-kernel components so that the gradient structure is maintained on the coarse grid.

3 Refinement-based Coarse Variables In this section, we construct the coarse variables and the resulting interpolation operator by following the geometric refinement of the mesh. To motivate the construction of R and S , we begin with the curl-curl problem on a uniform quadrilateral mesh shown in Figure 3.1a. The arrows indicate the orientation of the fine edges. Each degree of freedom corresponds to the tangential component along an oriented edge. Following geometric refinement, we can partition these 12 DoFs into the 8 external DoFs highlighted in blue and the remaining 4 interior DoFs. Specifically, each coarse edge is interpolated from two fine edges in the same blue circle and they represent the support of the two nonzeros in a row of R .

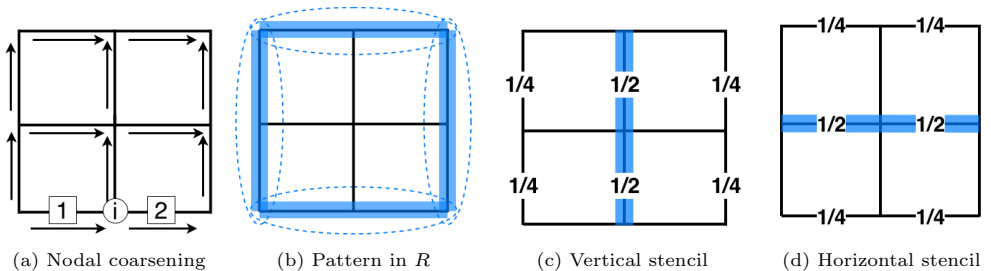


Fig. 3.1: Curl-curl on uniform quadrilateral mesh.

We now focus on the bottom coarse edge in Figure 3.1a, formed by the two fine edges DoFs labeled 1 and 2 meeting at the node i . The i -th column of the discrete gradient G , restricted to these two edge DoFs (after normalization), is

$$\frac{1}{\sqrt{2}} [1 \quad -1]^T,$$

with signs determined by the edge orientations in the figure. We assign this vector as a column of S , placing these entries on DoFs 1 and 2 and zeros elsewhere. Since

R and S must be orthogonal, the corresponding row of R must be the orthogonal complement of $\frac{1}{\sqrt{2}} [1, -1]^T$. We use the simplest choice

$$\frac{1}{\sqrt{2}} [1 \quad 1].$$

If one of the fine edges has an opposite orientation, the signs in both R and S must be flipped consistently according to G . To span the remaining interior space, we assign corresponding Euclidean basis vectors as columns in S . S and R admit the following block representations

$$(3.1) \quad S = [S_I \quad S_E], \quad R = [0 \quad R_E],$$

where the subscripts I and E denote the interior Euclidean bases and the exterior pairs, respectively.

In this special case of Figure 3.1a, where the two fine edges have consistent orientation, our choice of R_E and S_E coincides with the choice in Theorem 6.2 of [2]. In that setting, the coarse variables are defined purely to ensure orthogonality between R and S , namely,

$$R_E = \frac{1}{\sqrt{2}} [I \quad I], \quad S_E = \frac{1}{\sqrt{2}} [I \quad I]$$

However, this choice does not explicitly incorporate the orientation induced by the G . Consequently, the resulting interpolation doesn't preserve the commuting in Equation 3.4 in general. In contrast, our construction preserves near-kernels, as we show in the following section.

3.1 Sparse approximation of the ideal interpolation To obtain a sparse approximation of the ideal interpolation defined in Equation 1.5, we retain S_I and drop S_E in S . Intuitively, we drop S_E^T because the exterior DoFs are already represented by the coarse variables in R^T , and so the interpolation reduces to a harmonic extension from the exterior into the interior. This leads to the sparse approximation

$$(3.2) \quad P_{\text{app}} := (I - S_I(S_I^T A S_I)^{-1} S_I^T A) R^T = (I - \Pi_A(S_I)) R^T,$$

an interior A -harmonic extension of the gradient-preserving coarse variables. This truncation yields a sparse approximation of the ideal interpolation operator because $S^T A S$ is simplified to $S_I^T A S_I = A_{II}^{-1}$. Moreover, the interior blocks are local and, by construction, decoupled from the exterior variables. As a result, A_{II}^{-1} can be computed using independent local block inverses.

We first show a crucial fact induced by our interior/exterior structural design. Notation-wise, we write the interior/exterior splitting of A and G as

$$A = \begin{bmatrix} A_{II} & A_{IE} \\ A_{EI} & A_{EE} \end{bmatrix}, \quad G = \begin{bmatrix} G_I \\ G_E \end{bmatrix}.$$

Let $X_E(A) = A_{EE} - A_{EI} A_{II}^{-1} A_{IE}$ be the Schur complement of A on the exterior.

LEMMA 3.1. *Assume the stiffness interior block A_{II}^* is invertible. Then*

$$X_E(A^*) S_E = 0.$$

Proof. Let \mathbf{s} be any column of S_E . By construction, there exists a column \mathbf{g} of G whose exterior restriction equals \mathbf{s} , namely,

$$\mathbf{g} = \begin{bmatrix} \mathbf{g}_I \\ \mathbf{s} \end{bmatrix} \quad \text{for some } \mathbf{g}_I.$$

By the exact sequence (2.2), we have $A^s \mathbf{g} = \mathbf{0}$. Writing this in block form gives

$$A_{II}^s \mathbf{g}_I + A_{IE}^s \mathbf{s} = \mathbf{0}, \quad A_{EI}^s \mathbf{g}_I + A_{EE}^s \mathbf{s} = \mathbf{0}.$$

Since A_{II}^s is invertible,

$$\mathbf{g}_I = -(A_{II}^s)^{-1} A_{IE}^s \mathbf{s}.$$

Substituting for \mathbf{g}_I in the exterior equation yields the Schur complement on the exterior

$$(A_{EE}^s - A_{EI}^s (A_{II}^s)^{-1} A_{IE}^s) \mathbf{s} = \mathbf{0} \quad \text{or} \quad X_E(A^s) \mathbf{s} = \mathbf{0}$$

Since this holds for each column of S_E , we conclude $X_E(A^s) S_E = \mathbf{0}$. \square

By the same argument, $X_E(A^s) G_E = \mathbf{0}$ also holds. Now, we are ready to present the main results. Following the GAMG framework [2], the weak approximation property for P_{app} is implied once the corresponding coarse-grid projection satisfies the approximate harmonic property [2, (4.1)]. The next theorem establishes this property for P_{app} with the unshifted curl-curl operator A^s . Since $\beta = 0$, P_{app} reduces to

$$P_{\text{app}} = (I - S_I (A_{II}^s)^{-1} S_I^T A^s) R^T$$

THEOREM 3.2 (Approximate harmonic property for P_{app}). *Let P_\star and P_{app} be defined as above, and set $Q_\star := P_\star R$ and $Q_{\text{app}} := P_{\text{app}} R$. Assume that Q_\star satisfies the approximate harmonic property [2, (4.1)], i.e., there exists $\eta_\star \geq 1$ such that*

$$\|Q_\star \mathbf{e}\|_{A^s} \leq \sqrt{\eta_\star} \|\mathbf{e}\|_{A^s} \quad \text{for all } \mathbf{e} \in \mathbb{R}^n.$$

Then Q_{app} also satisfies [2, (4.1)] with

$$\|Q_{\text{app}} \mathbf{e}\|_{A^s} \leq \sqrt{\eta_{\text{app}}} \|\mathbf{e}\|_{A^s} \quad \text{for all } \mathbf{e} \in \mathbb{R}^n,$$

where $\eta_{\text{app}} \geq 1$.

Proof. By the triangle inequality,

$$\|Q_{\text{app}} \mathbf{e}\|_{A^s} \leq \|Q_\star \mathbf{e}\|_{A^s} + \|(P_{\text{app}} - P_\star) R \mathbf{e}\|_{A^s}.$$

Since Q_\star satisfies the approximate harmonic property, it suffices to bound the second term. A block computation gives

$$P_{\text{app}} - P_\star = \begin{bmatrix} -A_{II}^s & -1 & A_{IE}^s \\ & & I \end{bmatrix} \Pi_{X_E(A^s)}(S_E) R_E^T.$$

Since $\Pi_{X_E(A^s)}(S_E)$ is a projector,

$$\|\Pi_{X_E(A^s)}(S_E) \mathbf{e}\|_{X_E(A^s)} \leq \|\mathbf{e}\|_{X_E(A^s)}.$$

Moreover, a direct calculation shows

$$\left\| \begin{bmatrix} -A_{II}^s & -1 & A_{IE}^s \\ & & I \end{bmatrix} \mathbf{e} \right\|_{A^s} = \|\mathbf{e}\|_{X_E(A^s)}.$$

Hence,

$$\begin{aligned}
\|(P_{\text{app}} - P_{\star})\mathbf{R}\mathbf{e}\|_{A^s} &= \left\| \begin{bmatrix} -A_{II}^s & -1 & A_{IE}^s \\ & I & \end{bmatrix} \Pi_{X_E(A^s)}(S_E) R_E^T \mathbf{R}\mathbf{e} \right\|_{A^s} \\
&\leq \left\| \Pi_{X_E(A^s)}(S_E) R_E^T \mathbf{R}\mathbf{e} \right\|_{X_E(A^s)} \\
&\leq \|R_E^T \mathbf{R}\mathbf{e}\|_{X_E(A^s)} \\
&= \|(I - S_E S_E^T) \mathbf{e}_E\|_{X_E(A^s)} \\
&\leq \|\mathbf{e}_E\|_{X_E(A^s)} + \|S_E S_E^T \mathbf{e}_E\|_{X_E(A^s)} \\
&= \|\mathbf{e}_E\|_{X_E(A^s)} \leq \|\mathbf{e}\|_{A^s}
\end{aligned}$$

The fourth line uses the identity $R_E^T R_E = I - S_E S_E^T$, since $R_E^T R_E$ is a projection onto $\text{range}(R_E^T)$ and $S_E S_E^T$ is the complementary projection. The term $\|S_E S_E^T \mathbf{e}_E\|_{X_E(A^s)}$ vanishes by lemma 3.1. The last inequality follows by direct computation. Finally, it follows that $\sqrt{\eta_{\text{app}}} \leq 1 + \sqrt{\eta_{\star}}$. \square

We now discuss the commuting relation for P_{app} . We first need to define the coarse grid gradient G_C . It is natural to obtain the coarse gradient by projecting the fine gradient onto the coarse edge space. Accordingly, we set

$$(3.3) \quad G_C := R G I_C,$$

where I_C is an injection operator in the nodal space that selects all nonzero columns of $R G$.

THEOREM 3.3 (Commuting property for P_{app}). *There exists a nodal interpolation operator P_n such that the commuting relation holds*

$$(3.4) \quad P_{\text{app}} G_C = G P_n$$

for the unshifted case $\beta = 0$.

Proof. It suffices to show that the columns of $P_{\text{app}} G_C$ lie in $\ker(A^s)$. Then, a direct block computation yields

$$A^s P_{\text{app}} G_C = A^s (I - \Pi_{A^s}(S_I)) R^T R G I_C = \begin{bmatrix} 0 \\ X_E(A^s) R_E^T R_E G_E I_C \end{bmatrix}.$$

Again, by $R_E^T R_E = I - S_E S_E^T$, we can rewrite

$$\begin{aligned}
X_E(A^s) R_E^T R_E G_E I_C &= X_E(A^s) (I - S_E S_E^T) G_E I_C \\
&= X_E(A^s) G_E I_C - X_E(A^s) S_E (S_E^T G_E I_C).
\end{aligned}$$

Both terms vanish by Lemma 3.1. \square

This shows that such nodal interpolation P_n exists, but we don't derive its explicit form because we don't use it in our multilevel construction. Different from [7, 9], where the commuting relation is derived from explicit topological constraints, our commuting arises naturally from the harmonic extension. A key advantage of the refinement-based approach is that it can recover exact refinement transfer. In particular, we have consistently observed numerically that our refinement-based interpolation reduces to geometric interpolation on isotropic curl-curl problems. In the example of

Figures 3.1a–3.1b, the sparse approximation (3.2) yields the geometric interpolation stencils shown in Figures 3.1d–3.1c, up to an $O(\beta)$ perturbation. In more general jump-coefficient settings, the method incorporates coefficient variations directly into the interpolation while preserving a clear geometric hierarchy.

Finally, we note that the invertibility of A_{II}^s is not automatic. For the shifted curl-curl operator with $\beta \neq 0$, the weak approximation property and the commuting relation are no longer exact. However, our analysis and numerical experiments indicate that the defect term is small and scales linearly with β . Consequently, the commuting relation and the weak approximation property of P_{app} remain valid up to an $O(\beta)$ perturbation, which vanishes in the limit $\beta \rightarrow 0$. A fully rigorous treatment of the singular limit and the associated generalized Schur complement remains the subject of ongoing work.

4 Fully Algebraic Coarsening In section 3, we introduced a refinement-based AMG algorithm that takes advantage of the hierarchical geometric structure to build a sparse interpolation. The key ingredient was an interior/exterior splitting together with a local harmonic extension that preserves near-kernel components. In this section, we extend this strategy to a fully algebraic setting. The interpolation continues to take the form in Eq. (3.2). Thus, the main task is to construct the interior/exterior splitting algebraically in order to define the coarse variables R^T and interior Euclidean basis S_I .

The following steps summarize the two-level setup:

1. Augment the gradient matrix $\tilde{G} = \text{augment}(G)$ to recover boundary nodes.
2. Form and coarsen $A_{\tilde{G}} = \tilde{G}^T A \tilde{G}$.
3. Construct the coarse and fine variables and compute the interpolation operator P_{app} .
4. Define the coarse-level gradient $G_c = RGI_c$.

We describe each step in detail below.

4.1 Nodal coarsening Although the curl-curl operator is discretized with edges DoFs, we begin the algebraic construction by coarsening a dual nodal space. The motivation is that nodes are naturally associated with gradients. By nodal coarsening, we implicitly select which gradient components are represented on the coarse grid. Moreover, nodal coarsening serves as an intermediate step that determines the endpoints of the support of the coarse-level gradient. These endpoints, in turn, define exterior edge variables by connecting edge DoFs between them.

To formalize this idea, we first define the nodal dual operator

$$A_G = G^T A G.$$

A_G determines the effective coupling between the discrete gradient components induced by the fine level operator A . Its graph structure reflects the strength of interaction among local gradient modes and guides the selection of nodal DoFs that approximate the gradients on the coarse level.

However, a drawback of A_G is that it does not fully capture the local connectivity near the boundary, particularly under Dirichlet boundary conditions. Recall that each row of G corresponds to an edge, and each column corresponds to a nodal DoF. An interior edge row has exactly two nonzeros. A boundary edge, however, has only one adjacent node in the domain, resulting in a single nonzero entry. Consequently, A_G does not reflect the nodal adjacency near the boundary. To restore the boundary structure, we augment G by appending an additional column for every boundary node

so that each boundary edge is associated with two nodal entries of opposite sign. This modification preserves the signed-incidence structure of the gradient operator and ensures that the corresponding augmented nodal dual operator

$$A_{\tilde{G}} = \tilde{G}^T A \tilde{G}$$

encodes a consistent nodal graph across both the interior and the boundary. Algorithm 4.1 is presented below. Note that the boundary-node indices \mathcal{B} are artificial and serve only to restore boundary connectivity.

Algorithm 4.1 augment G with boundary-node columns

```

1: function AUGMENTG( $G$ )
    $\tilde{G} = G$ ,  $m =$  number of columns of  $G$ ,  $k = 0$ 
2: for  $i = 1, 2, \dots$ , number of rows of  $G$  do
3:   if  $\text{nnz}(G(i, :)) = 1$  then ▷  $i$  is a boundary edge-row
4:     Let  $\delta$  be the unique nonzero value in row  $G(i, :)$ 
5:      $k \leftarrow k + 1$ 
6:      $\tilde{G} = \begin{bmatrix} \tilde{G} & [0 \ \dots \ [-\delta]_i \ \dots \ 0]^T \end{bmatrix}$ 
7:   end if
8: end for
9:    $\mathcal{B} := \{m + 1, m + 2, \dots, m + k\}$ 
10: return  $\tilde{G}$ ,  $\mathcal{B}$ 
11: end function

```

We now perform a classical C/F splitting on $A_{\tilde{G}}$ to select a coarse subset of nodal unknowns. In the scope of this paper, we mark all nearest neighbors of coarse nodes as fine nodes. The subsequent construction of the exterior/interior splitting is formulated consistently with this choice. More aggressive nodal coarsening would require a modified strategy for constructing exterior paths and is therefore left for future research. Algorithm 4.2 describes this coarsening process. We denote the set of neighbors of a DoF b in the graph of A by $\mathcal{N}_A(b) := \{j \neq b : (A)_{bj} \neq 0\}$.

Algorithm 4.2 C/F splitting for $A_{\tilde{G}}$ with prescribed boundary nodes

```

1: function NODALCF( $A$ ,  $\tilde{G}$ ,  $\mathcal{B}$ )
    $A_{\tilde{G}} = \tilde{G}^T A \tilde{G}$ ,  $\mathbf{c} = \mathcal{B}$ ,  $\mathbf{f} = \emptyset$ 
2: for  $b \in \mathcal{B}$  do
3:    $\mathbf{f} \leftarrow \mathbf{f} \cup \mathcal{N}_{A_{\tilde{G}}}(b)$ 
4: end for
5:  $(\mathbf{c}, \mathbf{f}) \leftarrow$  C/F splitting( $A_{\tilde{G}}$ ;  $C_{\text{ini}} = \mathbf{c}$ ,  $F_{\text{ini}} = \mathbf{f}$ )
6:  $\mathbf{c}_{\mathbf{G}} \leftarrow \mathbf{c} \setminus \mathcal{B}$  ▷ coarse set excluding boundary nodes
7:  $\mathbf{f}_{\mathbf{G}} \leftarrow \mathbf{f}$ 
8: return  $\mathbf{c}_{\mathbf{G}}$ ,  $\mathbf{f}_{\mathbf{G}}$ 
9: end function

```

In this algorithm, the boundary-node indices \mathcal{B} are prescribed as the initial coarse nodes, and their neighbors are marked as initial fine nodes (line 5). We then apply classical C/F splitting to the remaining interior nodal DoFs. Setting \mathcal{B} as coarse nodes ensures that algebraic exterior paths can extend naturally to the boundary

whenever needed in the later edge construction. Moreover, this choice helps maintain a structured and geometrically consistent exterior/interior splitting.

4.2 Algebraic construction of coarse and fine variables Having obtained the coarse nodal set \mathbf{c}_G , we now construct the coarse and fine variables in the edge space, namely R and S . The goal is to algebraically reproduce the refinement-based interior/exterior splitting introduced in Section 3. We achieve this by using the nodal coarsening as an auxiliary tool for pairing edge DoFs.

In particular, \mathbf{c}_G determines the endpoints of algebraic length-two paths. For each pair of coarse nodes $i, j \in \mathbf{c}_G$ that are distance-two neighbors in the nodal graph induced by $A_{\tilde{G}}$, we identify a mutual distance-one neighbor k . The edge path connecting $i \rightarrow k \rightarrow j$ select two fine edge DoFs, denoted $\{DoF_1, DoF_2\}$. We then form a coarse edge variable, or equivalently a row in R , by averaging these two DoFs with signs consistent with the orientation stored in G . All remaining edge DoFs are classified as the interior and form a Euclidean basis S_I . This completes the interior/exterior splitting of the edge space. Algorithm 4.3 summarizes the full construction.

Algorithm 4.3 construct the interpolation P

```

1: function FORMP( $A, G$ )
    $R = \emptyset$ ,  $\mathbf{dof} = \{1, \dots, n\}$ ,  $\mathcal{K} = \emptyset$ 
2:  $\tilde{G}, \mathcal{B} \leftarrow \text{augmentG}(G)$ 
3:  $\mathbf{c}_G, \mathbf{f}_G \leftarrow \text{nodalCF}(A, \tilde{G}, \mathcal{B})$ 
4:  $\mathbf{c}_G \leftarrow \mathbf{c}_G \cup \mathcal{B}$  ▷ allow paths to boundary nodes
5: for  $(i, j) \in \mathbf{c}_G \times \mathbf{c}_G$ ,  $i < j$  do
6:   if  $i, j$  are distance-two neighbors and  $(i, j) \notin \mathcal{B}$  then
7:      $k \leftarrow$  a mutual distance-one neighbor of  $i, j$ 
8:     if  $k \notin \mathcal{K}$  then ▷ enforce unique distance-2 path
9:       Select  $\{DoF_1, DoF_2\} \subset \mathbf{dof}$  connecting  $i \rightarrow k \rightarrow j$ 
10:       $\mathbf{dof} \leftarrow \mathbf{dof} \setminus \{DoF_1, DoF_2\}$ 
11:       $\mathcal{K} \leftarrow \mathcal{K} \cup \{k\}$ 
12:      Construct  $r$  with  $\text{supp}(r) = \{DoF_1, DoF_2\}$  and entries  $\pm 1$ 
13:       $R^T \leftarrow [R^T \ r]$ 
14:     end if
15:   end if
16: end for
17:  $S_I \leftarrow I(:, \mathbf{dof})$  ▷  $S_I^T A S_I = A_{II}$ 
18: return  $P_\star = R^T - S_I A_{II}^{-1} (S_I^T A R^T)$ 
19: end function

```

We now make several important remarks on the design of Algorithm 4.3. First, the existence of distance-two paths is a direct consequence of the nodal coarsening strategy, which marks all nearest neighbors of coarse nodes as fine. As a result, coarse nodes are typically separated by exactly one intermediate fine node, which makes selecting length-two paths $i \rightarrow k \rightarrow j$ available. Second, line 4 ensures that interior coarse nodes can form distance-two paths that extend to the boundary. Since all boundary nodes were initially prescribed as coarse in Algorithm 4.2, interior coarse nodes can connect to boundary nodes whenever a valid path exists. This design choice helps maintain a structural coarse-edge pattern. Third, the condition $(i, j) \notin \mathcal{B}$ in line 6 ensures a unique path between coarse nodes. This reduces grid complexity while

preserving a structured coarse-level gradient.

We emphasize that the algebraically constructed interpolation operator retains the key properties in Theorem 3.2 and Theorem 3.3. Line 10 enforces distinct edge DoFs in different rows of R , which preserves the orthogonality between R and S . Moreover, line 8 ensures that only one path passes through one intermediate gradient. The set \mathcal{K} keeps a record of which intermediate gradients, or intermediate fine nodes, have been used. By ensuring that each intermediate node participates in at most one path, we satisfy

$$X_E(A^s) S_E = 0,$$

which is an essential condition for establishing the commuting relation in Theorem 3.3.

To illustrate the construction, we apply Algorithm 4.3 to curl-curl on some sample uniform meshes. The results are shown in Figure 4.1. The red circles mark the coarse nodes, and blue denotes the distance-two paths that define the exterior variables in R .

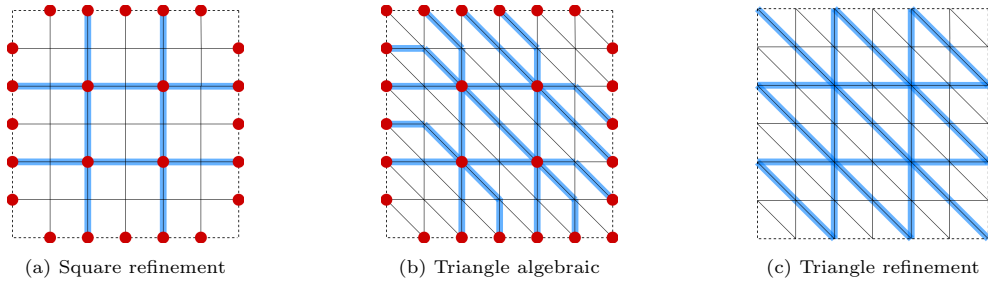


Fig. 4.1: uniform meshes with Dirichlet boundary conditions

Figure 4.1a shows that, on a uniform square mesh, the algebraic splitting coincides exactly with geometric refinement. In general, the algebraic construction does not recover geometric refinement exactly. This is illustrated in the uniform triangular mesh case, where Figure 4.1b differs from the geometric refinement shown in Figure 4.1c. Nevertheless, the algebraic splitting still produces highly structured gradients in the coarse grid. Moreover, as demonstrated in Section 5, the resulting convergence rates are very close.

Finally, we form the coarse-level gradient $G_C = RGI_C$ in the multilevel hierarchy. For algebraic coarsening, $I_C = I_{\mathbf{c}_G}$, the injection operator on the coarse nodes.

5 Numerical Results We present numerical experiments for the curl-curl model problem discretized with lowest-order Nédélec edge elements. We evaluate the multilevel performance of the proposed sparsified ideal interpolation operators P_{app} , constructed using both geometric refinement and fully algebraic splitting via Algorithm 4.3, and compare them with the geometric Nédélec interpolation. We test both isotropic and jump configurations. All experiments use a V-cycle multilevel method with one pre- and one post-smoothing step. The smoother we use is a symmetrized multiplicative Schwarz relaxation followed by an ℓ_1 -Jacobi iteration (OSS- ℓ_1). The shift is set to $\beta = 0.01$ throughout. The stopping criteria is relative residual with a tolerance 10^{-8} . We set a maximum of 20 AMG levels and a minimum coarse grid size of 32 DoFs for the algebraic coarsening. We report both standalone AMG V-cycle iteration counts and the preconditioned conjugate gradient (PCG) iteration counts, along with the operator complexity (OC), with respect to the refinement level L and

the problem size n . We use a randomly generated initial guess and a deterministic right-hand side $b = (1, 2, \dots, n)^T$. We denote the three different interpolations in the tables as follows: “Geo” for geometric Nédélec interpolation, “Ref” for refinement-based sparsified ideal interpolation, and “Alg” for sparsified ideal interpolation generated algebraically by algorithm 4.3.

Table 5.1: Uniform triangular mesh

L	n	AMG			PCG			OC		
		Geo	Ref	Alg	Geo	Ref	Alg	Geo	Ref	Alg
4	736	22	22	25	8	8	7	1.29	1.29	1.28
5	3,008	23	23	25	8	8	7	1.31	1.31	1.31
6	12,160	22	22	24	8	8	7	1.32	1.32	1.32
7	48,896	21	21	24	8	8	7	1.33	1.33	1.33
8	196,096	23	23	25	7	7	7	1.33	1.33	1.33

First, we test the isotropic problem on uniform triangular meshes in Table 5.1. This serves as a baseline to show that all three interpolations do not degrade performance on nice, regular meshes. Numerically, we observe that refinement-based sparsified ideal interpolation recovers the geometric Nédélec interpolation up to β in isotropy, and thus it is not surprising that it exhibits the same iteration count and operator complexity. Our fully algebraic interpolation also yields nearly identical iteration counts and operator complexities, which suggests that the algebraic splitting produces a multilevel hierarchy that closely mimics the refinement in this setting.

Table 5.2: Uniform triangular mesh with jumps

L	n	AMG			PCG			OC		
		Geo	Ref	Alg	Geo	Ref	Alg	Geo	Ref	Alg
4	736	80	8	33	11	5	7	1.29	1.29	1.28
5	3,008	182	11	35	17	5	7	1.31	1.31	1.31
6	12,160	278	12	33	24	5	7	1.32	1.32	1.32
7	48,896	320	13	35	26	5	6	1.33	1.33	1.33

Next, in Table 5.2, we consider discontinuous jumps in $\mu(x)$ on the same meshes, where the jump coefficient alternates between 10 and 0.1 with every vertical line of elements on the fine grid. This creates increasingly frequent high-contrast jumps and introduces strong misalignment between the coefficient interfaces in the multilevel hierarchy, making it a particularly challenging test for multigrid. In contrast to the isotropic case, the geometric Nédélec interpolation exhibits a clear deterioration in both the standalone AMG and PCG performance as the mesh refines. This is expected since pure geometric transfer does not capture coefficient variations across the interface. On the other hand, both the refinement-based sparsified ideal interpolation and the fully algebraic construction remain robust across refinements. This is because their A -orthogonal construction incorporates the jump coefficients directly into the interpolation operator and thus adapts to variations across interfaces. As a result, the iteration counts remain nearly uniform under refinement. Importantly, the operator complexity of the algebraic construction remains similar to that of refinement, showing that its robustness does not come at the expense of increased hierarchy cost.

Finally, we consider discontinuous jumps on a set of Delaunay triangulations of the unit square. Different from 5.2, the jump regions are fixed in space and do not increase with refinement. The coarsest level is an unstructured Delaunay mesh illustrated in 5.1a, and we refine uniformly in each subsequent level. In addition to mesh irregularity, the unstructured distribution of jump regions poses a further challenge.

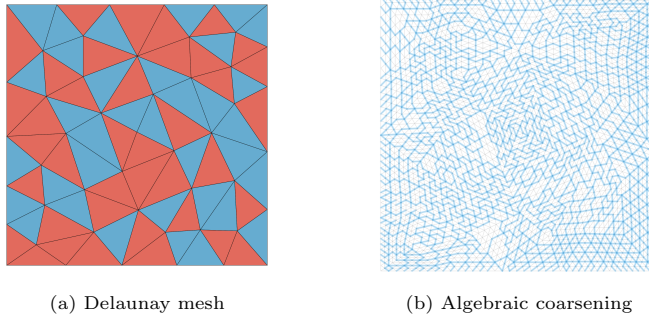


Fig. 5.1: Unstructured Delaunay test. Left: piecewise-constant jump coefficients, $\mu = 0.1$ in red and $\mu = 10$ in blue. Right: finest level algebraic coarse variable pattern on $L = 3$.

Table 5.3: Delaunay mesh with jumps

L	n	AMG			PCG			OC		
		Geo	Ref	Alg	Geo	Ref	Alg	Geo	Ref	Alg
3	7,024	96	7	132	23	6	23	1.32	1.32	1.44
4	28,256	67	7	321	21	6	37	1.33	1.33	1.92
5	113,344	47	8	400	20	6	53	1.33	1.33	3.22

Table 5.4: Delaunay mesh with jumps—two level

L	n	AMG			PCG			OC		
		Geo	Ref	Alg	Geo	Ref	Alg	Geo	Ref	Alg
3	7,024	23	7	9	10	6	7	1.24	1.24	1.26
4	28,256	14	7	9	9	6	7	1.25	1.25	1.29
5	113,344	13	7	10	9	6	7	1.25	1.25	1.31

Table 5.3 clearly shows that refinement-based interpolation significantly outperforms the geometric interpolation. The iteration counts for the geometric interpolation decrease under refinement because, as the mesh is refined, the relative influence of the jump interface reduces. This refinement dependence reflects its sensitivity to the jump coefficient distribution. In contrast, the constant iteration counts of the refinement-based interpolation demonstrate strong mesh independence. Moreover, its performance is insensitive to the irregular mesh geometry, the location of the jump regions, and the high jump coefficient contrast. This confirms that preserving the near-kernel structure through the refinement construction leads to robust multilevel convergence. However, the purely algebraic construction performs substantially worse

in this unstructured setting. Both the operator complexity and the iteration counts increase noticeably with refinement. Nevertheless, the encouraging two-grid results of the same problem in Table 5.4 suggest that the algebraic coarsening framework has clear potential. In particular, the algebraic construction there exhibits iteration counts and operator complexities comparable to the refinement-based method, and they remain uniform across refinement. This suggests that the performance degrades rapidly after the second level. As illustrated in Figure 5.1b, the algebraic coarsening on the finest mesh of $L = 3$ leaves several large interior fine regions uncoarsened. These regions cause large coupling within the interior blocks, which then transfers to the corresponding coarse operators through the Galerkin projection. The same mechanism repeats on subsequent levels, leading to more coupling and rapid growth in operator complexity. This suggests that further refinement of the coarsening strategy is needed to better adapt to unstructured mesh geometry and prevent the formation of large interior fine blocks.

6 Conclusions This work is the first H(curl) AMG construction derived directly from the GAMG framework, offering a harmonic-extension-based alternative to classical topological and global energy-minimization approaches. Based on an interior/exterior splitting, we developed interpolation strategies in both a refinement-based and a fully algebraic setting. We established the theoretical foundation of this approach, including the weak approximation property and the commuting relation. Numerical results demonstrate the robustness of the refinement-based interpolation, which consistently outperforms geometric interpolation in strong, spatially varying jump problems. The fully algebraic construction shows promising behavior, although further improvements are needed to achieve optimal performance on highly unstructured meshes. Ongoing work focuses on strengthening the algebraic hierarchy and extending the framework to three-dimensional problems.

REFERENCES

- [1] J. BRANNICK, F. CAO, K. KAHL, R. D. FALGOUT, AND X. HU, *Optimal interpolation and compatible relaxation in classical algebraic multigrid*, SISC, 40 (2018), pp. A1473–A1493.
- [2] R. D. FALGOUT AND P. S. VASSILEVSKI, *On generalizing the AMG framework*, SINUM, 42 (2004), pp. 1669–1693. UCRL-JC-150807.
- [3] R. D. FALGOUT, P. S. VASSILEVSKI, AND L. T. ZIKATANOV, *On two-grid convergence estimates*, Numer. Linear Algebra Appl., 12 (2005), pp. 471–494. UCRL-JRNL-203843.
- [4] R. HIPTMAIR, *Multigrid method for maxwell's equations*, SINUM, 36 (1998), pp. 204–225.
- [5] R. HIPTMAIR, *Finite elements in computational electromagnetism*, Acta Numerica, 11 (2002), pp. 237–339.
- [6] J.C.NEDELEC, *Mixed finite elements in r^3* , Numerische Mathematik, 35 (1980), pp. 315–341.
- [7] S. REITZINGER AND J. SCHÖBERL, *An algebraic multigrid method for finite element discretizations with edge elements*, Numerical linear algebra with applications, 9 (2002), pp. 223–238.
- [8] J. W. RUGE AND K. STÜBEN, *Algebraic multigrid (AMG)*, in Multigrid Methods, S. F. McCormick, ed., Frontiers Appl. Math., SIAM, Philadelphia, 1987, pp. 73–130.
- [9] R. TUMINARO AND C. GLUSA, *A structure preserving h-curl algebraic multigrid method for the eddy current equations*, arXiv preprint arXiv:2506.08284, (2025).